Nanchung and Inactive define pore properties of the native auditory transduction channel in *Drosophila*

Bingxue Li[a,b,1], Songling Li[a,b,1], Honglan Zheng[a,b], and Zhiqiang Yan[a,b,2]

[a]State Key Laboratory of Medical Neurobiology and MOE Frontiers Center for Brain Science, Institute of Brain Science, School of Life Sciences, Fudan University, Shanghai 200438, China; and [b]Institute of Molecular Physiology, Shenzhen Bay Laboratory, Shenzhen 518132, China

Edited by Rachel I. Wilson, Harvard Medical School, Boston, MA, and approved October 26, 2021 (received for review April 6, 2021)

Auditory transduction is mediated by chordotonal (Cho) neurons in *Drosophila* larvae, but the molecular identity of the mechanotransduction (MET) channel is elusive. Here, we established a whole-cell recording system of Cho neurons and showed that two transient receptor potential vanilloid (TRPV) channels, Nanchung (NAN) and Inactive (IAV), are essential for MET currents in Cho neurons. NAN and IAV form active ion channels when expressed simultaneously in S2 cells. Point mutations in the pore region of NAN-IAV change the reversal potential of the MET currents. Particularly, residues 857 through 990 in the IAV carboxyl terminus regulate the kinetics of MET currents in Cho neurons. In addition, TRPN channel NompC contributes to the adaptation of auditory transduction currents independent of its ion-conduction function. These results indicate that NAN-IAV, rather than NompC, functions as essential pore-forming subunits of the native auditory transduction channel in *Drosophila* and provide insights into the gating mechanism of MET currents in Cho neurons.

auditory transduction | mechanotransduction ion channel | TRP channel | patch clamp recording | *Drosophila* larvae

Drosophila is endowed with specialized auditory receptor cells in which sound waves are transduced into electrical signals. However, the key molecules/ion channels mediating this mechanotransduction (MET) process remain obscure. In adult flies, Johnston's organ neurons (JONs) detect sound and gravity (1–5). At the tip of the dendrite, each JON bears a cilium, in which the auditory transduction takes place. Two transient receptor potential (TRP) channels, Nanchung (NAN) and Inactive (IAV), are both localized to the proximal cilia (6), while NompC has a restricted distribution in the distal cilia (7). All three molecules are the potential candidates mediating the MET currents in JONs.

NAN and IAV are required for sound sensation in JONs (6, 8, 9). Furthermore, NAN and IAV are expressed in auditory receptor neurons and likely function as heteromers (6, 8). In *nan* or *iav* null mutants, the compound action potential induced by sound is abolished (6, 8). In addition, NompC is a mechanosensitive channel responsible for touch sensation in *Drosophila* (7). Importantly, the antennal sound receivers in *nompC* null allele mutant show no nonlinear amplification to pure tone stimuli. Moreover, self-sustained oscillations of antennal sound receivers are abolished in *nompC* null mutant (10), but it is still unclear whether NAN, IAV, and NompC amplify subthreshold MET current or mediate the subthreshold MET current themselves in auditory receptor neurons (1, 10–13). Therefore, it is necessary to study the following: first, whether NAN, IAV, and NompC are essential for the primary MET current evoked by sound; furthermore, which of them are the pore-forming subunits of the native auditory transduction channel; and finally, the gating mechanism of MET currents.

Patch clamp recordings of JONs are not feasible, because these neurons are very small and their cell bodies are embedded in a delicate antenna whose integrity is crucial for their function (13). Thus, we established patch clamp recordings of chordotonal (Cho) neurons of *Drosophila* larvae and showed that NAN and IAV are essential for the MET current in Cho neurons. We further found that NAN and IAV form active ion channels when coexpressed in heterologous cells. Mutations in the pore lining residues of NAN and IAV altered the permeation properties of native MET current in Cho neurons. We also identified residues 857 through 990 in the IAV carboxyl terminus that regulate the adaptation time constant of MET currents. Additionally, *nompC* null mutants showed a decreased adaptation time constant of the MET current, with the current amplitude comparable to that in wild-type. Moreover, a nonconducting point mutation of NompC did not affect MET currents. These findings provide convincing evidence that NAN-IAV channels form the pore of the native auditory transduction channel in *Drosophila* and reveal functional domains in NAN and IAV for channel gating. Intriguingly, NompC regulates auditory transduction currents independent of its ion-conducting function, which is consistent with the idea that NompC couples forces to the transduction channels by acting as the amplifier.

Results

Direct Patch Clamp Recording of the MET Current in Cho Neurons in *Drosophila* Larvae. A primary difficulty in resolving the roles of NAN and IAV in *Drosophila* auditory transduction has been the fact that patch clamp recordings of JONs are not feasible. To address this issue, in the current study, we developed the patch clamp recording of Cho neurons in *Drosophila* larvae, which

Significance

Chordotonal (Cho) neurons are responsible for auditory perception in *Drosophila*, but the molecules/ion channels mediating the primary subthreshold currents that transduce the sound/mechanical stimulation to electrical signal remain unclear. Here, we overcame the technical limitation of direct recording from auditory receptor neurons and explored the functions of candidate molecules in auditory transduction. The mechanically induced subthreshold currents showed high sensitivity, dose-dependent response, and desensitization characteristics. By analyzing point mutations, we revealed that the TRP channels Nanchung and Inactive are essential pore-forming subunits of the native auditory transduction channel in Cho neurons. Additionally, another TRP family member, NompC, plays a role in regulating the kinetics of auditory transduction currents.

Author contributions: B.L., S.L., and Z.Y. designed research; B.L., S.L., and H.Z. performed research; B.L. and S.L. analyzed data; and B.L., S.L., and Z.Y. wrote the paper.

The authors declare no competing interest.

This article is a PNAS Direct Submission.

[1]B.L. and S.L. contributed equally to this work.

[2]To whom correspondence may be addressed. Email: zqyan@szbl.ac.cn.

This article contains supporting information online at http://www.pnas.org/lookup/suppl/doi:10.1073/pnas.2106459118/-/DCSupplemental.

Published November 30, 2021.

enabled us to measure the subthreshold mechanosensitive current in Cho neurons directly. Each abdominal hemisegment of *Drosophila* larvae contains a cluster of five Cho neurons (lch5) and three singlet Cho neurons (vchA, vchB, and lch1) (14). We chose lch1 neurons in abdominal segments 2 through 6 for all the recordings. Similar to previous studies in vertebrate hair cells (15–20), we used a sealed and polished glass probe to deliver mechanical stimuli driven by a piezo actuator. Using previously established extracellular recordings (14), we found that the number of mechanical stimuli–induced spikes of lch1 neurons increased progressively with increasing stimulation strength (*SI Appendix*, Fig. S1). A displacement to the tip of the dendrite by 200 nm was found to be sufficient to increase spikes in lch1 neurons, and the response was already saturated at 1 μm (*SI Appendix*, Fig. S1). After removing the body wall muscles covering the Cho neurons, a tight seal was accomplished, and then the membrane was broken with suction to achieve whole-cell recording (Fig. 1*A*). To confirm the identity of Cho neurons unambiguously, we added Alexa Fluor 568 or neurobiotin to the pipette solution. The morphology of the targeted neurons loaded with neurobiotin was visualized by post hoc staining with streptavidin-cy3 (Fig. 1*D*). Consistent with previous studies on insect auditory receptor neurons (21, 22), Cho neurons exhibited spontaneous depolarizations of varying amplitude (Fig. 1*B*). Upon the onset and removal of mechanical stimuli, we observed both "on" and "off" current responses (Fig. 1*B*). The peak amplitude of the "on" current is −80.26 ± 6.14 pA (Fig. 1*E*). The response current had an activation time constant of 1.39 ± 0.17 ms and a latency of 3.46 ± 0.68 ms (Fig. 1*C*). The latency of MET currents in our study is evidently longer than those measured in vertebrate hair cells (23, 24), raising the possibility that activation of the transduction channel in flies is not direct, and it is possible that other as-yet-unknown second messengers with matching onset kinetics might be involved. The "on" response exhibited a slightly larger current amplitude than the "off" response (Fig. 1*E*). After reaching the peak response, the response current displayed a fast adaptation time constant (3.58 ± 0.34 ms), and the adaptation time constants of the "on" and "off" responses showed no

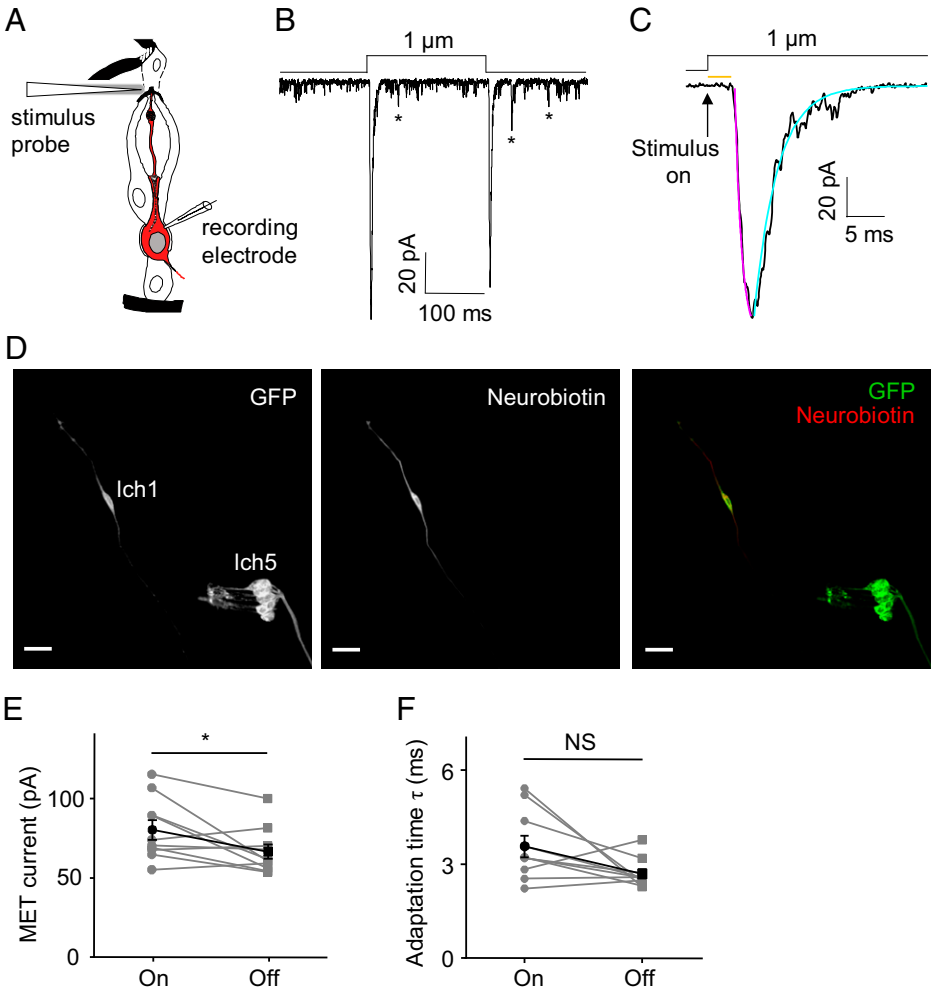

Fig. 1. Current responses of Cho neurons to mechanical stimuli. (*A*) Schematic illustrating the patch clamp recording preparation of Cho neurons; the illustration of Cho neurons was adapted from ref. 2. Copyright [2000] Society for Neuroscience. A glass probe driven by a piezo actuator was used to deliver mechanical stimuli to the tip of the lch1 Cho neuron dendrite. The cell in red is the lch1 neuron. (*B* and *C*) The whole-cell current in lch1 neurons was evoked by a 1-μm stimulus. The asterisks mark the spontaneous discrete depolarizations. The "on" response current is shown in *C* at a higher time resolution. The arrow represents the onset of the stimulus. The orange line indicates the response latency of the MET current. The purple line represents a single exponential fit of the activation of MET currents; the cyan line represents a single exponential fit of the adaptation of MET currents. (*D*) Post hoc immunostaining of the targeted neuron loaded with neurobiotin. *Iav-Gal4* was utilized to drive the expression of GFP in Cho neurons. (Scale bar, 15 μm.) (*E* and *F*) The amplitudes of the "on" and "off" current are shown in *E* ($n = 10$; paired t test). The peak values (absolute value) are used here. The adaptation time constants (τ) are summarized in *F* ($n = 10$; paired t test). All error bars denote ± SEM. $^*P < 0.05$; NS, not statistically significant. The holding potential was −60 mV, and the MET current was recorded in extracellular Na^+/intracellular K^+-based solutions. Genotype is as follows: *Iav-Gal4*/+; *UAS-CD8-GFP*/+.

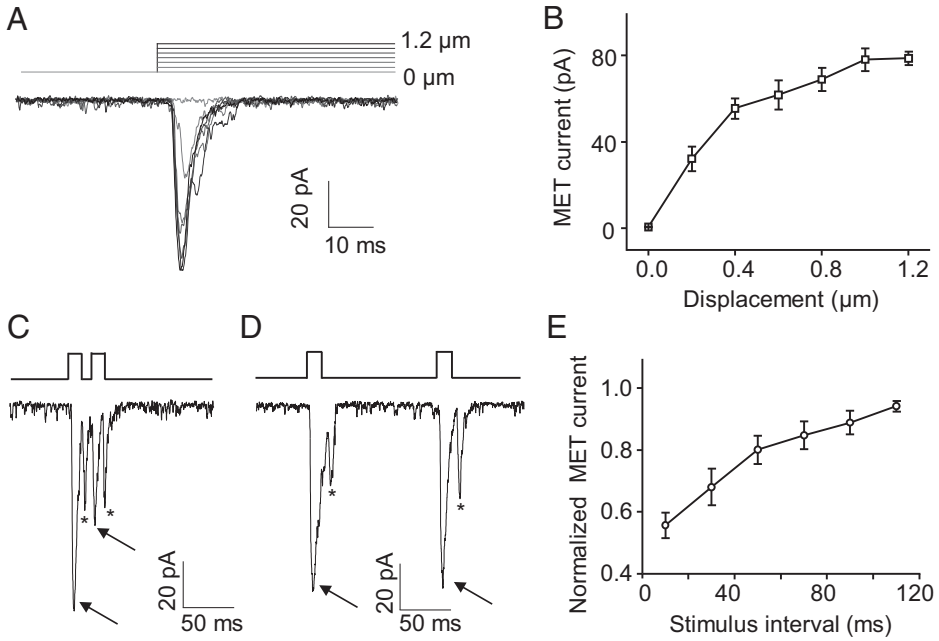

Fig. 2. Dose-dependent effect and desensitization characteristics of MET currents in Cho neurons. (*A*) Representative traces recorded from a lch1 neuron in response to 0.2-, 0.4-, 0.6-, 0.8-, 1.0-, and 1.2-μm displacements. (*B*) The MET currents (absolute value) increased with increased displacements. $n = 6$ for each displacement. The displacements were 0, 0.2, 0.4, 0.6, 0.8, 1.0, and 1.2 μm. All error bars denote ± SEM. (*C* and *D*) Representative traces of MET currents in lch1 in response to repetitive stimuli with a short (10 ms) and long (110 ms) interval. One mechanical stimulus evoked both "on" and "off" responses; arrows and asterisks represent the "on" and "off" response currents, respectively. (*E*) Summary of the amplitude of MET currents evoked by repetitive stimuli with different intervals ranging from 10 ms to 110 ms with 20-ms increments (mean ± SEM; $n = 6$ for each group). The lch1 neuron was clamped at −60 mV (holding potential) in Na^+/K^+-based solutions.

significant difference (Fig. 1*F*). Based on these characteristics of MET currents, the "on" response currents were analyzed in the following experiments.

Dose-Dependent Response and Desensitization Characteristics of MET Currents in Cho Neurons. We applied increased displacements to the cilia of lch1 neurons and found that the amplitude of MET currents increased progressively (Fig. 2 *A* and *B*). Similar to the vertebrate hair cells (15–20), lch1 neurons can sense deflection in the nanometer range. This sensitivity could provide *Drosophila* larvae sufficient ability to detect vibration or sound. Combining the results of extracellular recordings, 1-μm displacement was used in the following whole-cell recordings to induce the MET currents. To identify whether the MET currents undergo desensitization, we applied repetitive stimuli to lch1 neurons. MET currents in lch1 neurons appeared to desensitize with shorter intervals and progressively lose desensitization to repeated stimuli with longer intervals (Fig. 2 *C–E*), similar to the mechanoreceptor currents in worm cephalic neurons (25).

Both NAN and IAV Are Essential for the MET Currents in Cho Neurons. The ability to record whole-cell currents of lch1 neurons enables us to analyze whether NAN and IAV channels carry the MET currents of Cho neurons. First, we found that nan^{36a} mutant larvae had no detectable response to 1-μm displacement (Fig. 3*A*). We then used *Iav-Gal4* to drive the *UAS-NAN-GFP* transgene in the nan^{36a} mutants. The lch1 neurons of the *nan* rescued larvae showed MET currents comparable to those of wild-type larvae, with similar response amplitude (−80.38 ± 6.09 pA), activation time constant (1.33 ± 0.10 ms), and adaptation time constant (4.17 ± 0.79 ms) (Fig. 3 *A–D*). We further analyzed the characteristics of MET currents in an *iav* null mutant (iav^1) by the same preparation. The current induced by 1-μm displacement was also abolished (Fig. 3*A*) and was rescued by the expression of IAV-GFP in the iav^1 mutants (Fig. 3 *A–D*). In addition, in both the *nan* and *iav* mutants, we increased the displacement up to 5 μm, which was larger than the saturation stimulus, and the response was still undetectable (*SI Appendix*, Fig. S2). Similarly, the lch1 neurons in iav^1 and nan^{36a} mutants did not show sound-evoked transduction currents upon exposure to a 500-Hz pure tone, though the sound intensity had increased to 90 dB SPL (*SI Appendix*, Fig. S3). These results demonstrate that NAN and IAV are both essential for primary MET currents in Cho neurons.

NAN and IAV Simultaneously Expressed in *Drosophila* S2 Cells Form Active Cation Channels. We then tested whether NAN and IAV could form functional channels in a heterologous expression system. To tackle this problem, we first transfected *Drosophila* S2 cells with NAN or IAV alone and found no channel events (*SI Appendix*, Fig. S4). Then, we analyzed the S2 cells cotransfected with both NAN and IAV and found spontaneous channel openings in whole-cell recordings (Fig. 4*A*). This result is consistent with the idea that NAN and IAV both contribute to a heteromeric ion channel in auditory transduction (6). A previous study revealed a large current induced by nicotinamide (NAM) in oocytes expressing both NAN and IAV (26). Here, we found that NAM could stably increase the opening probability of NAN-IAV channels in S2 cells (Fig. 4 *B* and *D* and *SI Appendix*, Fig. S5). We detected typical single-channel activity; the all-event amplitude histogram plotted from NAN-IAV single-channel currents showed two peaks (Fig. 4*C*). Traces of channel opening revealed individual channels with an amplitude of ~20.13 ± 0.51 pA at −60 mV, comparable to spontaneous channel openings without NAM (20.83 ± 1.73 pA) (Fig. 4*E*), so we added 2 μM NAM in internal solution to conduct the following experiments on S2 cells. Further, we found that *Drosophila* S2 cells transfected with NAN or IAV alone still showed no channel events by adding NAM to the internal solution (*SI Appendix*, Fig. S6). Under voltage steps, NAN-IAV

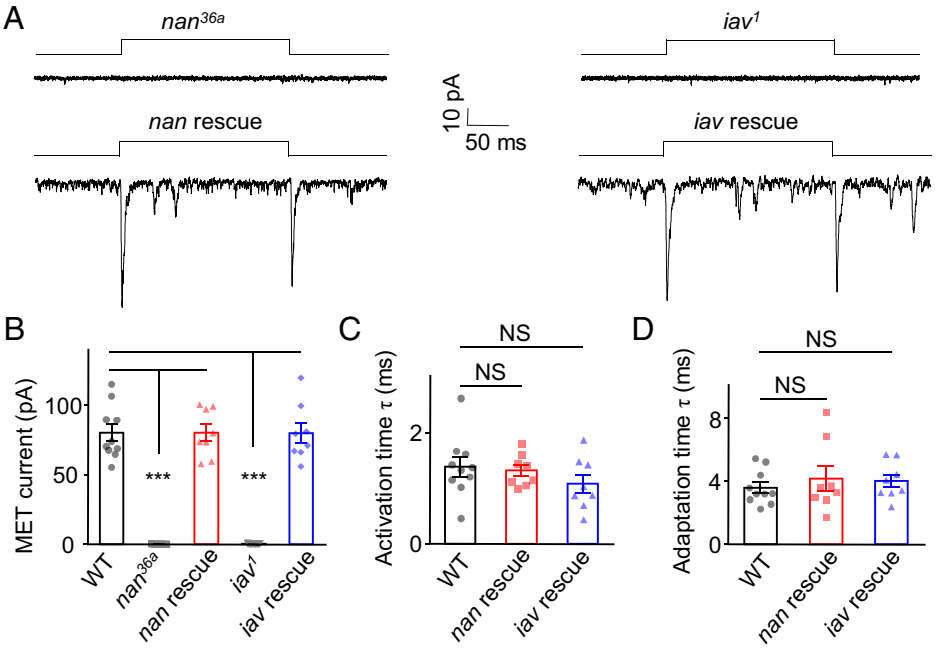

Fig. 3. NAN and IAV are required for mechanical stimuli–induced whole-cell current in lch1 Cho neurons. (*A*) Current response to a mechanical stimulus (1 μm) was eliminated in *nan* and *iav* null mutants but could be rescued by expressing NAN and IAV in lch1 neurons of nan^{36a} and iav^{1} mutants, respectively. Lch1 neurons were clamped at −60 mV (holding potential) in Na^+/K^+-based solutions. (*B*) Bar graph summarizing the peak current (absolute value) of the lch1 neurons in wild-type (WT), nan^{36a}, *nan* rescue, iav^{1}, and *iav* rescue larvae (n = 10, 7, 8, 9, and 8, respectively; mean ± SEM). (*C*) The activation time constants of MET currents in larvae with indicated genotype (n = 10, 8, 8, respectively, mean ± SEM). (*D*) Summary of the adaptation time constants of MET currents in WT, *nan* rescue, and *iav* rescue larvae (n = 10, 8, and 8, respectively; mean ± SEM). The unpaired t test was used for comparison between two groups, and one-way ANOVA followed by Holm–Šidák post hoc analysis was used for comparison among multiple groups. ***$P < 0.001$. NS, not statistically significant. Genotypes are as follows: nan^{36a}: *Iav-Gal4/UAS-GFP*; nan^{36a}/nan^{36a}. iav^{1}: iav^{1}/y; *Iav-Gal4/+*; *UAS-CD8-GFP/+*. *nan* rescue: *Iav-Gal4, UAS-GFP/UAS-Nanchung-GFP*; nan^{36a}/nan^{36a}. *iav* rescue: iav^{1}/y; *Iav-Gal4, UAS-GFP/+*; *UAS-Inactive-GFP/+*. WT: *Iav-Gal4/+*; *UAS-CD8-GFP/+*.

showed a linear I–V relationship in Na^+/K^+ solutions and the single-channel conductance of NAN-IAV was 315.43 ± 4.27 pS at −64.5 mV (*SI Appendix*, Fig. S7). Then, we found that NAN-IAV channels exhibited a slightly higher permeability to K^+ than to Na^+ (P_{Na^+}/P_{Cs^+} = 0.84 ± 0.03; P_{K^+}/P_{Cs^+} = 1.06 ± 0.03), whereas the Ca^{2+} permeability was significantly higher ($P_{Ca^{2+}}/P_{Cs^+}$ = 2.18 ± 0.19) (Fig. 4 *F–I* and *SI Appendix*, Fig. S8), which was consistent with the properties of TRP family ion channels.

Next, we tested whether NAN-IAV could be activated by mechanical forces. Based on our previous study of mechanosensitive channel NompC (7), we used the same recording and stimulus protocol. NompC displayed obvious response currents to mechanical displacements and negative pressure; however, NAN-IAV showed no response to these stimuli in S2 cells (*SI Appendix*, Fig. S9). Considering NAN-IAV might be tuned to different types of mechanical forces compared with NompC, we tested the effects of positive pressure on NAN-IAV. However, no response currents were recorded (*SI Appendix*, Fig. S9). These results indicate that NAN-IAV may not respond to mechanical stimuli directly and that some other proteins may sense the forces, which, in turn, help gate NAN-IAV in auditory transduction.

Mutations in the Putative Selectivity Filter of NAN-IAV Alter the Reversal Potential of MET Currents in Cho Neurons. To further demonstrate that NAN-IAV forms the pore of the auditory transduction channel, we examined the ion selectivity of the MET current by introducing point mutations in the predicted pore region of NAN-IAV. The structure of rat transient receptor potential vanilloid subtype 1 (TRPV1) was resolved, and the pore and ion permeation pathway of TRPV1 was clearly revealed (27, 28). Based on the sequence homology among *Drosophila* NAN, *Drosophila* IAV, and rat TRPV1 channels, we mutated negatively charged residues near the putative selective filter region of NAN and IAV (Fig. 5*A*). We found that point mutations NAN-D681A and IAV-D615A both shifted the reversal potential of NAN-IAV channels in S2 cells (*SI Appendix*, Fig. S10). This observation suggests that the mutated residues are located near the channel pore of NAN-IAV. Then, each of the GFP-tagged constructs harboring point mutations was expressed in lch1 neurons of the nan^{36a} or iav^{1} mutants. The MET currents of Cho neurons from the nan^{D681A} and iav^{D615A} mutants exhibited shifted reversal potentials by ∼14 mV and ∼21 mV, respectively (Fig. 5 *B–G*). These results demonstrate that mutations in the pore region of NAN and IAV altered the biophysical properties of the transduction channel in Cho neurons. Behaviorally, the transgenic larvae (nan^{D681A} and iav^{D615A}) showed lower responses to 500 Hz pure tone stimulation than wild-type larvae, as the nan^{D681A} and iav^{D615A} mutations showed reduced MET currents at negative potentials (Fig. 5 *F* and *H*). Alteration of reversal potentials of transduction currents in sensory cells by putative pore mutation is the key evidence for determination of pore subunits of transduction channels (25, 29, 30). In summary, our findings suggest that NAN and IAV define pore properties of the native auditory transduction channel in *Drosophila*.

The Carboxyl Terminus of IAV Is Essential for Proper Localization of NAN-IAV Channels and Contributes to the Adaptation Time of MET Currents. Several studies suggest that N-terminal domains are involved in the gating mechanism of mechanically activated ion channels (31–34). Particularly, the 29 Ankyrin repeats (ARs) in the N terminus of NOMPC form a cytoplasmic domain required for NOMPC mechanogating in S2 cells and touch responses in *Drosophila* larvae (32, 33). Considering that NAN and IAV are also members of the *Drosophila* TRP channel family, we first evaluated the function of N-terminal ARs in the

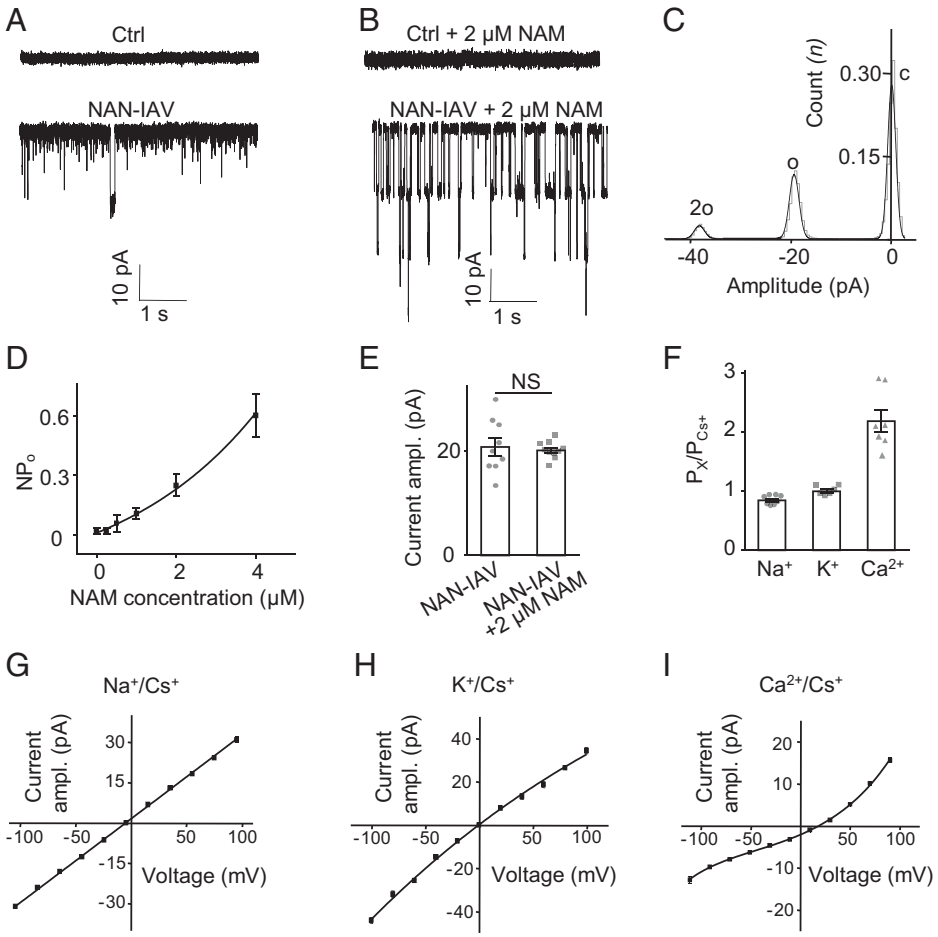

Fig. 4. NAN and IAV could form functional channels when expressed simultaneously in *Drosophila* S2 cells. (*A*) Representative traces of spontaneous channel activities in control and Inactive-mCherry– and Nanchung-Flag–coexpressing S2 cells at −60 mV (holding potential) in Na^+/K^+-based solutions. (*B*) Representative traces of single-channel activities in control and Inactive-mCherry– and Nanchung-Flag–coexpressing S2 cells at −60 mV (holding potential) in Na^+/K^+-based solutions with 2 μM NAM in internal solution. (*C*) Histogram showing activity of NAN-IAV single-channel currents with NAM. The black line indicates the Gaussian fit for the histogram. (*D*) The open probability of NAN-IAV channels with different concentrations of NAM in internal solution (mean ± SEM; n = 12, 8, 7, 9, 13, and 5 in each group). NP_o indicates the total open probability of active NAN-IAV channels. (*E*) Comparison of the current amplitude (absolute value) of spontaneously active NAN-IAV channels and NAM-induced channels at −60 mV (holding potential) in Na^+/K^+-based solutions. NAN-IAV, spontaneous current (n = 9); NAN-IAV+ 2 μM NAM (n = 10). Mean ± SEM, unpaired t test. NS, not statistically significant. (*F*) Permeability ratios of different cation combinations (n = 8, 6, and 7; mean ± SEM). "X" means Na^+, K^+, or Ca^{2+}. (*G*) Average current–voltage relationship of NAN-IAV single-channel currents in the bi-ionic extracellular Na^+/intracellular Cs^+ condition with NAM (n = 8; mean ± SEM). (*H*) Single-channel I–V curves of NAN-IAV in extracellular K^+/intracellular Cs^+ condition with NAM (n = 6; mean ± SEM). (*I*) Single-channel I–V curves of NAN-IAV in extracellular Ca^{2+}/intracellular Cs^+ conditions with NAM (n = 7; mean ± SEM).

gating of NAN-IAV (*SI Appendix*, Fig. S11). We generated six truncation constructs of NAN or IAV with deletion of each AR and then tested their single-channel activities in S2 cells. No single-channel activities were detected when deleting each single AR of either NAN or IAV (*SI Appendix*, Figs. S12 and S13). These results showed that N-terminal ARs of NAN or IAV are essential for proper channel activity, thus preventing us from further testing the involvement of N-terminal ARs in the NAN-IAV gating.

Second, we tested the role of the carboxyl terminus in the gating of the MET channel in lch1 neurons. Through analysis of NAN and IAV and their orthologs in other species, we found that the 857-1123 residues in the carboxyl-terminal region of IAV do not align with the TRPV1 channels in vertebrates and consist of a unique sequence (*SI Appendix*, Fig. S11). Because vertebrate TRPV1 channels do not play a role in MET, we speculate that this unique carboxyl-terminal region may play an important role in the mechanogating of NAN-IAV. First, we generated a truncation construct of IAV with the ΔC terminus (857-1123 residues) and tested its single-channel activities. When expressed in S2 cells, this truncated NAN-IAV showed a single-channel current identical to that exhibited by the full-length channel (Fig. 6 *A* and *C*). This result suggests that our truncation construct preserved active single-channel activity. Meanwhile, by nonpermeabilized immunostaining of the S2 cells, we confirmed the proper targeting of this mutant to the plasma membrane (*SI Appendix*, Fig. S14). Next, we asked whether MET currents in lch1 neurons could be affected when the IAV carboxyl terminus was deleted. By expressing IAV carboxyl-terminal truncation by the *Iav-Gal4* driver in the *iav* null mutant background, we noted that Δ857-1123-IAV-GFP does not localize to proximal cilia, unlike wild-type IAV (Fig. 6*D*). Consistent with the above result, Δ857-1123-IAV exhibited no MET currents in lch1 neurons (*SI Appendix*, Fig. S15*A*). These results demonstrate that precise localization of IAV is required for the normal function of Cho neurons. Furthermore, the IAV carboxyl terminus forms a domain that plays a critical role in IAV trafficking.

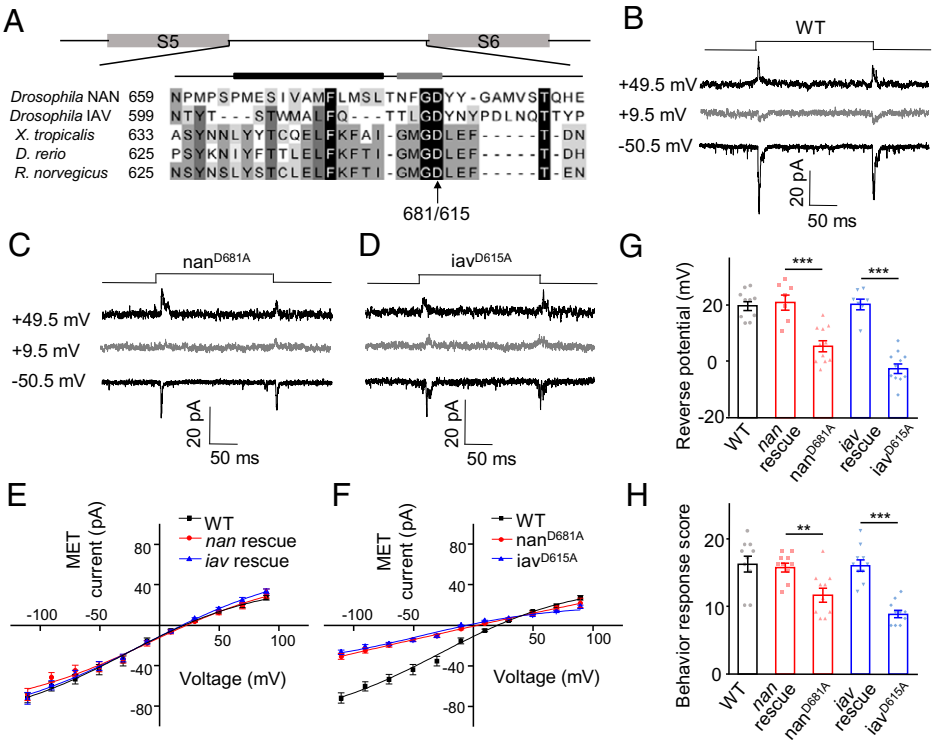

Fig. 5. Point mutations of NAN and IAV in selective filter regions shifted the reversal potential of MET current. (*A*) Sequence alignment of the putative pore regions of NAN and IAV and their homologs. The arrow marks the negatively charged residue Asp mutated to Ala. The putative pore helix (black bar, *Left*) and selectivity filter (gray bar, *Right*) are indicted above the sequences. (*B–D*) Representative traces of current responses to 1-μm displacement in wild-type and two selectivity filter mutants (nan^{D681A} and iav^{D615A}). Lch1 neurons were recorded in extracellular Na^+/intracellular Cs^+-based solutions with TEA. (*E*) Average current–voltage relationship of MET currents recorded from wild-type, *nan* rescue, and *iav* rescue larvae. Lch1 neurons were recorded in Na^+/Cs^+-based solutions (mean ± SEM; n = 10, 7, and 7, respectively). (*F*) I–V relations of MET currents in lch1 neurons of nan^{D681A} (n = 11) and iav^{D615A} (n = 11). MET currents of the wild-type were used in each graph for comparison. Lch1 neurons were recorded in Na^+/Cs^+-based solutions. All error bars denote ± SEM. (*G*) The reversal potential of MET currents in lch1 neurons recorded from larvae with the indicated genotype (mean ± SEM; n = 10, 7, 11, 7, and 11). (*H*) Summary of behavioral response of transgenes encoding wild-type and mutant forms of *nan* and *iav* (n = 10 for each group). The sound stimulus was 500 Hz pure tone. The unpaired t test was used for comparison between two groups, and one-way ANOVA followed by Holm–Šidák post hoc analysis was used for comparison among multiple groups. $^{**}P < 0.01$; $^{***}P < 0.001$. Genotypes are as follows: nan^{D681A}: *Iav-Gal4, UAS-GFP/UAS-nanD681A-GFP*; *nan^{36a}/nan^{36a}*. iav^{D615A}: *iav^1/y*; *Iav-Gal4, UAS-GFP/+*; *UAS-iavD615A-GFP/+*. *nan* rescue: *Iav-Gal4, UAS-GFP/UAS-Nanchung-GFP*; *nan^{36a}/nan^{36a}*. *iav* rescue: *iav^1/y*; *Iav-Gal4, UAS-GFP/+*; *UAS-Inactive-GFP/+*. WT: *Iav-Gal4/+*; *UAS-CD8-GFP/+*.

Based on the results above, we generated two additional IAV truncations, Δ857-990-IAV and Δ991-1123-IAV, which both showed normal single-channel currents in S2 cells (Fig. 6 *B* and *C*). However, these two truncations exhibited distinct functional properties in lch1 neurons. Expressing Δ991-1123-IAV channels in Cho neurons of *iav^1* mutants did not restore MET current responses (*SI Appendix*, Fig. S15*B*), consistent with the loss of proper localization (Fig. 6*D*), while Δ857-990-IAV could be trafficked to the proximal cilia as the wild-type IAV (Fig. 6*D*). Notably, Cho neurons rescued by Δ857-990-IAV responded to the mechanical stimuli (Fig. 6*E*). Compared with wild-type currents, the MET currents of Δ857-990-IAV displayed a prolonged adaptation time constant (Fig. 6*G*), while the activation time constant and amplitude of MET current showed no significant difference (Fig. 6 *F* and *H*). To map domains in the IAV carboxyl terminus that are involved in IAV trafficking, we further divided the residues 991 to 1,123 of IAV into three parts and generated truncations. While Δ991-1036-IAV showed normal distribution on the dendritic cilia, residues 1,037 through 1,081 (45 amino acids [aa]) and residues 1,082 through 1,123 (42 aa) both turned out to be essential for the proper targeting of IAV (*SI Appendix*, Fig. S16). Taken together, these findings illustrate that region 857 through 990 residues of IAV could regulate the kinetics of the MET current, whereas residues 1,037 through 1,123 of IAV are essential to the trafficking of IAV.

NompC Regulates the Kinetics of MET Currents Independent of Its Ion-Conduction Function. The bona fide mechanosensitive channel NompC is localized to the distal cilia of Cho neurons (7) and is another candidate for the MET channel in auditory transduction. We therefore tested the role of NompC in auditory transduction. The *nompC* null mutants (*nompC$^{1/3}$*) showed MET currents with comparable amplitude and activation time constant to those in wild-type (Fig. 7 *A*, *D*, and *E*). Remarkably, the adaptation time constant of MET currents in *nompC$^{1/3}$* larvae was shorter than that in wild-type (Fig. 7 *A* and *F*). Next, we calculated the areas under "on" response curves at −60 mV, and the *nompC$^{1/3}$* mutant exhibited a smaller summation of the inward current (Fig. 7*G*). This alteration of MET currents in Cho neurons coincides with previous reports that *nompC* mutation affects the sound response in *Drosophila* larvae (14). In summary, NompC likely regulates the adaptation of MET currents in Cho neurons.

Then, we used *Iav-Gal4* to drive wild-type NompC expression in Cho neurons of *nompC$^{1/3}$* mutants and rescued the adaptation time constant change of MET currents (Fig. 7 *B*, *D–F*), which further confirms the role of NompC in the adaptation of MET currents. As previously reported, the NompC "pore dead" mutation, NompC-E1511K, did not show active currents when expressed in S2 cells (7). We expressed the *UAS-NompC-E1511K* constructs in *nompC$^{1/3}$* mutants by *Iav-Gal4* and recorded the MET currents

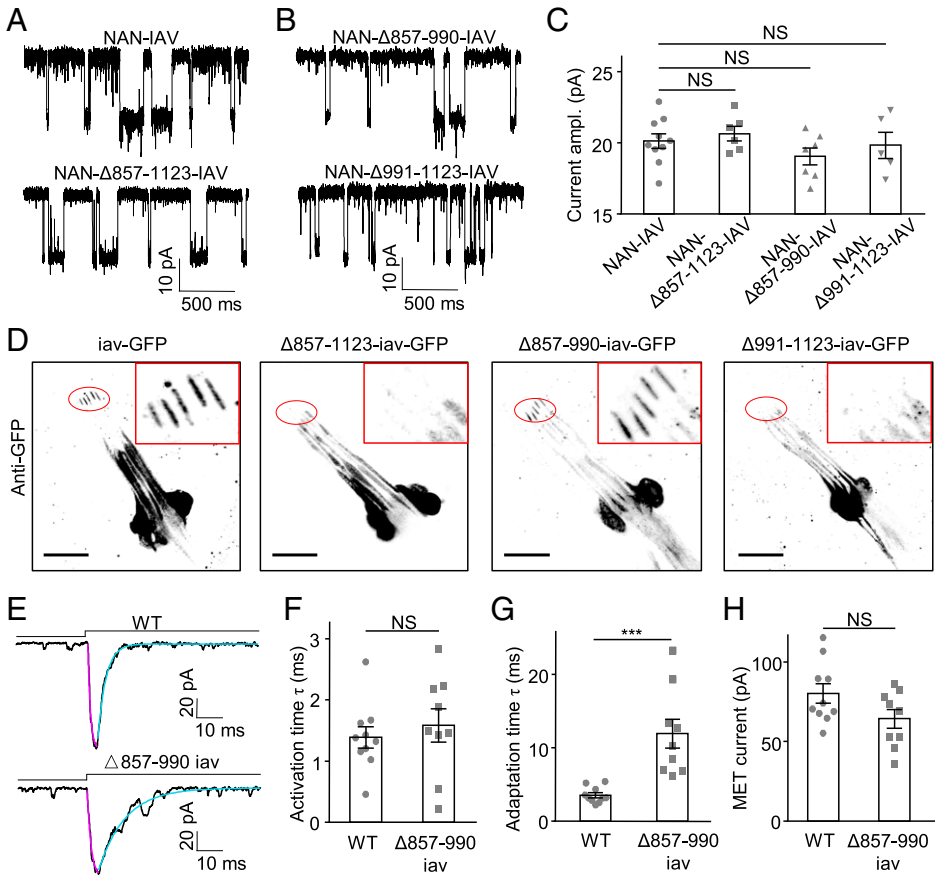

Fig. 6. The carboxyl-terminal region of IAV contributes to adaptation of MET currents and is essential for the proper localization of NAN-IAV channels. (*A* and *B*) Representative traces of single-channel activities in NAN-IAV–, NAN-Δ857-1123-IAV–, NAN-Δ857-990-IAV–, and NAN-Δ991-1123-IAV–expressing S2 cells with 2 μM NAM in internal solution. S2 cells were recorded at −60 mV (holding potential) in Na^+/K^+-based solutions. (*C*) Single-channel current amplitudes (absolute value) of wild-type and truncated NAN-IAV at −60 mV (holding potential) in Na^+/K^+-based solutions (n = 10, 6, 7, and 5; NS, not statistically significant). One-way ANOVA followed by Holm–Šidák post hoc analysis was used for comparison among multiple groups. (*D*) Wild-type and truncated IAV expression in Cho neurons of *iav*^{1} larvae. (Scale bar, 20 μm.) GFP signals are enhanced with an anti-GFP antibody (black). (*E*) Representative traces of MET current from wild-type and Δ857-990-iav larvae; lch1 neurons were held at −60 mV in Na^+/K^+-based solutions. Cyan lines represent single exponential fits of the adaptation of MET currents; purple lines represent single exponential fits of the activation of MET currents. (*F*) Deletion of 857-990 residues of IAV did not alter the activation time constant of MET currents in lch1 neurons (mean ± SEM, n = 10, 9; NS, not statisticlly significant, unpaired t test). (*G*) Deletion of 857-990 residues of IAV prolonged the adaptation time constant of MET currents (mean ± SEM, n = 10 and 9; ***$P < 0.001$, unpaired t test). (*H*) Summary of MET current amplitudes (absolute value) in lch1 neurons of wild-type and Δ857-990-iav larvae (mean ± SEM, n = 10 and 9; NS, not statistically significant, unpaired t test). Genotypes are as follows: for *D*, iav-GFP: *iav*^{1}/y; *Iav-Gal4*/+; *UAS-iav-GFP*/+. Δ857-1123-iav-GFP: *iav*^{1}/y; *Iav-Gal4*/+; *UAS-Δ857-1123-iav-GFP*/+. Δ857-990-iav-GFP: *iav*^{1}/y; *Iav-Gal4*/+; *UAS-Δ857-990-iav-GFP*/+. Δ991-1123-iav-GFP: *iav*^{1}/y; *Iav-Gal4*/+; *UAS-Δ991–1123-iav-GFP*/+. For *E-H*, Δ857-990-iav: *iav*^{1}/y; *Iav-Gal4*/+; *UAS-Δ857-990-iav-GFP*/+. WT: *Iav-Gal4*/+; *UAS-CD8-GFP*/+.

in Cho neurons. Strikingly, nompC^{E1511K} mutants showed MET currents with normal amplitude and kinetics (Fig. 7 *C–F*). Moreover, transgenic expression of wild-type NompC and NompC-E1511K mutation both restored sound-evoked startle response, while the *nompC*$^{1/3}$ mutant displayed attenuated response (Fig. 7*H*). These results suggest that NompC does not contribute to the conductance of the auditory transduction channel in *Drosophila*. Unexpectedly, the regulation of MET currents is independent of NompC's channel function. NompC may function as a structural protein in sound transduction through its unique 29 ARs (32, 35–37).

Discussion

The mechanism of auditory transduction in *Drosophila* has long been explored, and the primary question is the identification of transduction channels. Here, we established a whole-cell recording approach for Cho neurons in *Drosophila* larvae, allowing us to test the role of NAN, IAV, and NompC in auditory transduction.

Further recording of *nan* and *iav* mutants showed that NAN and IAV are essential for the MET currents of Cho neurons. Amino acid substitutions in the putative selectivity filter of NAN and IAV evidently shifted the reversal potential of MET currents. Furthermore, we identified the IAV carboxyl-terminal fragment (amino acids 1,037 through 1,123) required for IAV trafficking. Moreover, both the IAV carboxyl terminus (amino acids 857 through 990) and NompC regulated the adaptation kinetics of MET currents. Interestingly, the "pore dead" mutation NompC-E1511K did not affect the MET currents in Cho neurons. All these results indicate that *Drosophila* NAN and IAV, but not NompC, are pore-forming subunits of the native auditory transduction channel and highlight the function of the carboxyl terminus of IAV in the gating dynamics of the MET channel. In addition to *Drosophila* NOMPC (TRPN1) for gentle touch sensation, which we identified in a previous study (7), we show that TRP channels are the pore-forming subunits of sensory transduction channels in two major mechanosensation modalities in *Drosophila* larvae—touch and hearing.

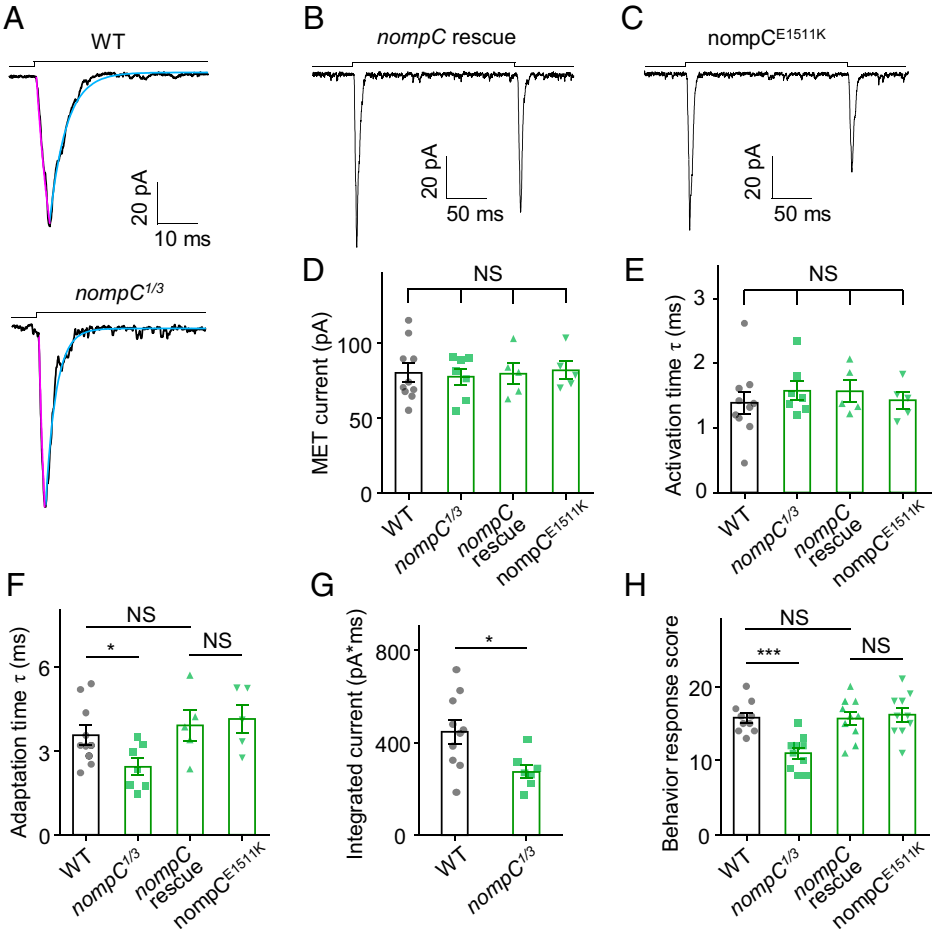

Fig. 7. NompC regulates the adaptation time of MET currents in Cho neurons. (*A*) Representative traces of MET currents from wild-type and *nompC*$^{1/3}$ null mutants. Cyan lines represent single exponential fits of the adaptation of MET currents; purple lines represent single exponential fits of the activation of MET currents. (*B* and *C*) Representative traces of MET currents from wild-type *nompC* rescue and nompC^{E1511K} mutant larvae. (*D*) Summary of MET current amplitudes (absolute value) of wild-type, *nompC*$^{1/3}$, *nompC* rescue, and nompC^{E1511K} (mean ± SEM, n = 10, 7, 5, and 5). (*E*) Activation time constants of MET current in wild-type, *nompC*$^{1/3}$, *nompC* rescue, and nompC^{E1511K} (mean ± SEM, n = 10, 7, 5, and 5; NS, not statistically significant). (*F*) Adaptation time constants of MET current in *nompC*$^{1/3}$ were smaller than those in wild-type, *nompC* rescue, and nompC^{E1511K} (mean ± SEM, n = 10, 7, 5, and 5). For *A*–*F*, Ich1 neurons were clamped at −60 mV (holding potential) in Na^+/K^+-based solutions. (*G*) Statistical analysis of integrated MET currents of wild-type and *nompC*$^{1/3}$ (mean ± SEM; n = 10 and 7). (*H*) Summary of behavioral response of wild-type, *nompC*$^{1/3}$, *nompC* rescue, and nompC^{E1511K} (n = 10 for each group). The sound stimulus was 500 Hz pure tone. The two-tailed unpaired t test was used for comparison between two groups, and one-way ANOVA followed by Holm–Šidák post hoc analysis was used for comparison among multiple groups. *P < 0.05; ***P < 0.001; NS, not statistically significant. Genotypes are as follows: WT: *Iav-Gal4/+*; *UAS-CD8-GFP/+*. *nompC*$^{1/3}$: *nompC*^{1}/*nompC*^{3}; *Iav-Gal4/UAS-CD8-GFP*. *nompC* rescue: *nompC*^{1}/*nompC*^{3}; *Iav-Gal4*, *UAS-CD8-GFP/UAS-nompC-GFP*. nompC^{E1511K}: *nompC*^{1}/*nompC*^{3}; *Iav-Gal4*, *UAS-CD8-GFP/UAS-nompC-E1511K-GFP*.

Mechanosensitive ion channels play critical roles in physiological functions such as touch, hearing, and gravity sensing (17, 38–41), and the gating mechanism of mechanosensitive ion channels, such as PIEZO, NOMPC, TRAAK, TMEM63/OSCA, and MSCL, is of extensive interest (31–33, 35, 42–50). As reported, NOMPC is gated by the cytoskeleton, and PIEZO, TRAAK, TMEM63/OSCA, and MSCL are gated by membrane tension (31–33, 35, 42–50). Compared with NOMPC and PIEZO, the MET channel of Cho neurons shows extreme sensitivity, which is of great interest (Fig. 2 *A* and *B*). The patch clamp recording of Cho neurons we developed in this study and the convenient genetics tools available for fruit flies provide a promising system to study the gating mechanism of the highly sensitive auditory transduction channels. Utilizing this system, we have shown that the unique carboxyl terminus of IAV plays important roles in the gating kinetics of the native auditory transduction channel, but critical questions regarding the mechanogating of these channels remain unclear.

Different from the reported mechanosensory transduction channels, NAN-IAV shows typical TRP channel characteristics but is not mechanosensitive when expressed in S2 cells. Thus, the further question is how NAN-IAV senses mechanical stimuli in Cho neurons. It is possible that NAN-IAV needs other cellular structure or accessory proteins to transduce the force in Cho neurons. NAN-IAV localizes in the proximal cilium of Cho neurons, and this cilium contains nine microtubular doublets and dynein arm–like protrusions (6, 8) (Fig. 6*D* and *SI Appendix*, Fig. S17), which are absent in S2 cells. Moreover, the *Drosophila* auditory organs rely on multiple accessory cells, which constitute the scolopidia together with Cho neurons (51–53), to transduce sound stimulus with high sensitivity (*SI Appendix*, Fig. S18). The cultured S2 cells have neither the ciliary structure nor scolopidia form; this might be the reason why NAN-IAV–related mechanosensitive currents could not be reconstituted in S2 cells. In addition, as a mechanosensitive channel, NompC also exists in the distal cilia of Cho neurons (7). Unexpectedly, in our recording system, NompC does not act as an ion-conducting pore of MET channels in Cho neurons (*SI Appendix*, Fig. S17). Considering that NompC owns unique 29 Ankyrin repeats (33) and these ARs could bind to the

microtubules, it probably functions as a structural protein (32, 35–37). NompC, microtubules, and dynein arms in the cilia probably work in concert with each other and participate in the force generation process of sound sensation.

It is also possible that NAN-IAV can be gated by other signals such as second messengers in the MET process in Cho neurons. It will be not surprising if NAN-IAV is gated or modulated by internal ligands, and this gating or modulation plays important roles in the MET process in Cho neurons. Whether other molecules control the gating of NAN-IAV needs more investigations. Importantly, resolving the structure of NAN-IAV will provide further insights into the gating mechanism, which is similar to NOMPC, PIEZO, TRAAK, TMEM63/OSCA, and MSCL (32, 42–48, 54–56).

Materials and Methods

***Drosophila* Lines.** The *Iav-Gal4*, *UAS-CD8-GFP*, *Nanchung* null mutant (*nan*^{36a}), and *Inactive* null mutant (*iav*^{1}) lines were obtained from the Bloomington Stock Center. The *UAS-GFP* line was a gift from Yongqing Zhang, Institute of Genetics and Developmental Biology, Chinese Academy of Sciences, Beijing, China. Flies were reared at room temperature (25 °C) in an incubator with 12-h light/dark cycles and 60% relative humidity control.

S2 Cell Culture and Transient Transfection. *Drosophila* S2 cells were cultured in Schneider's medium supplemented with 10% fetal bovine serum at 25 °C. Cells were plated into 35-mm Petri dishes before transfection. TransIT-Insect was used to transfect cells according to the product protocol (Mirus). Wild-type or mutated pUAST-IAV-mCherry and pUAST-NAN-Flag constructs were cotransfected with pActin-Gal4. Before recording, cells were plated onto ConA-coated coverslips in 35-mm Petri dishes. Recordings were carried out 1.5 to 2 d after transfection. Wild-type pUAST-NompC-EGFP were transfected with pActin-Gal4, and recordings were carried out 1 d after transfection.

Generation of Mutated NAN, IAV, and NompC Constructs. Full-length complementary DNAs of *nan* (NM_001274904.1) and *iav* (NM_132125.2) were synthesized from Genewiz, with the addition of a carboxyl-terminal Flag tag for NAN and a carboxyl-terminal fusion mCherry for IAV. The wild-type pUAST-NOMPC-EGFP vector was a gift from the Yuh Nung Jan Laboratory. Point mutations (NAN-D681A, IAV-D615A, and NompC-E1511K) were introduced into the coding sequence of *nan*, *iav*, and *nompC* through PCR-based site-directed mutagenesis in a pBluescript vector. To generate truncation constructs, a PCR-based approach was used. The fragment encoding amino acids of the targeted region was replaced by a linker of two alanine residues using a One-Step Cloning Kit (Vazyme Biotech). For S2 cell expression, the coding regions of wild-type and mutated NOMPC-EGFP, NAN-Flag, or IAV-mCherry were subcloned into a modified pUAST vector, which was simplified by removing the mini*white* element. All constructs were sequenced to validate the desired mutations.

Generation of Transgenic Flies. The coding regions of wild-type and mutant *nan*, *iav*, or *nompC* were subcloned into the pUAST-GFP vector with eGFP in-frame fused on the carboxyl terminus of the inserted sequence. Then, transgenic lines were generated by conventional P-element–mediated germ-line transformation in the Core Facility of *Drosophila* Resource and Technology (Shanghai Institute of Biochemistry and Cell Biology, Chinese Academy of Sciences).

Behavior Assay. According to a previous study (14), we placed a 2% agar plate (100 mm) on top of a speaker and adjusted the parameters to achieve a 90-dB pure tone (500 Hz). Third-instar larvae were gently collected, washed twice with phosphate-buffered saline (PBS), and transferred to the agar plate. After the larvae began to crawl freely, their behavior responses to sound stimuli were analyzed and recorded. To evaluate the larval sound response, the larvae were stimulated with a 1-s pure tone repeated 10 times. Sound stimulation could be applied only after each free crawl. Larvae that did not respond to sound were scored 0. A score of 1 was given to larvae that paused, those that retracted the mouth hook were scored 2, and those that retracted with excessive turning and/or backward locomotion were scored as 3. The sum of responses in 10 trials served as the response score. All the behavior tests were conducted at room temperature.

***Drosophila* Larval Dissection and Electrophysiological Recordings.** As previously described (7, 14), fillet preparations were performed by dissecting third-instar larvae in hemolymph-like saline (bath solution) containing (in millimolar): 103 NaCl, 3 KCl, 5 *N*-[Tris(hydroxymethyl)methyl]-2-aminoethanesulfonic acid, 10 trehalose, 10 glucose, 7 sucrose, 26 $NaHCO_3$, 1 NaH_2PO_4, and 4 $MgCl_2$, adjusted to pH 7.20 and 270 to 275 mOsm. Before use, 2 mM Ca^{2+} was added to the saline. The muscles covering the lch1 Cho neurons were gently removed with fine forceps, and lch1 neurons were exposed. The Cho neurons were visualized and identified by fluorescent markers driven by *Iav-Gal4*. Glass electrodes were pulled with a P-97 puller (Sutter Instrument) from thick wall borosilicate glass.

For extracellular recording, the recording electrodes were pulled to a diameter of ~3 μm and filled with external saline solution. For whole-cell recording, patch electrodes with 15 to 20 MΩ resistance were used. Except for the experiments to measure the current–voltage relationship, the pipette solution contained (in millimolar) 140 potassium aspartate, 10 Hepes, 4 MgATP, 0.5 Na_3GTP, 1 EGTA, and 1 KCl (pH = 7.20, adjusted to ~265 mOsm) (57). The pipette solution also contained Alexa Fluor 568 (1 μM), and the identity of the neuron was confirmed with dye fill. Meanwhile, 500 nM tetrodotoxin was added to the bath solution to reduce the occurrence of unclamped spikes (22, 58). Lch1 neurons were voltage clamped at −60 mV to analyze the characteristics of MET currents in lch1 neurons unless indicated otherwise. For the Na^+/K^+-based solutions for whole-cell recording of Cho neurons, the measured liquid junction potential was observed as +9.8 mV (59). For further detailed confocal visualization of axons and dendrites of individual recorded lch1 neurons, 0.5% neurobiotin was added to the recording pipette solution instead of the Alexa Fluor 568. After completing whole-cell recording, pulses of depolarizing current of 10~30 pA were injected with 150-ms duration at 3.3 Hz for 2 to 10 min to facilitate the entry of neurobiotin into the recorded neurons.

To measure the current–voltage relationship of MET currents in lch1 neurons, a Cs^+-based pipette solution was used to replace the K^+-based pipette solution. In addition, tetraethylammonium (TEA) (10 mM) was used to minimize the contributions of voltage-gated K^+ currents (58). This pipette solution contained (in millimolar) 140 cesium methanesulfonate, 10 Hepes, 4 MgATP, 0.5 Na_3GTP, 1 EGTA, 1 CsCl, and 10 TEA. For the current–voltage experiments in Cho neurons, the voltage command proceeded from −100 mV to +100 mV. The measured liquid junction potential for the current–voltage relationship for MET currents in lch1 neurons was observed as +10.5 mV (59).

The sampling rate was 20 kHz and filtered at 1 kHz (low-pass). A Multiclamp 200B amplifier, DIGIDATA 1550A, and Clampex 10.5 software (Molecular Devices) were used to acquire and process the data.

S2 Cell Electrophysiological Recordings. Whole-cell recordings of S2 cells were carried out under an Olympus BX51WI microscope equipped with a 40× water-immersion lens. Transfected cells were identified by fluorescence. Patch electrodes with 10 to 15 MΩ resistance were used. The pipette solution contained 140 mM potassium gluconic acid and 10 mM Hepes. The bath solution contained 140 mM NaMES (sodium methanesulfonate) and 10 mM Hepes. For ion selectivity experiments, the Cs^+ pipette solution contained 140 mM CsMES in bi-ionic conditions and 10 mM Hepes. The K^+ bath solution contained 140 mM potassium gluconic acid and 10 mM Hepes. The Ca^{2+} bath solution consisted of 70 mM CaMES, 10 mM Hepes, and 100 mM sucrose. All solutions were adjusted to 320 mOsm and pH 7.2. Unless otherwise indicated, all the pipette solutions contained 2 μM NAM. For the current–voltage experiments, the voltage command proceeded from −100 mV to +100 mV. The sample rate was 20 kHz and filtered at 1 kHz (low-pass). A multiclamp 200B amplifier, DIGIDATA 1550A, and Clampex 10.5 software (Molecular Devices) were used to acquire and process the data.

To record the effect of NAM on NAN-IAV single-channel activity, different concentrations were applied in the pipette solution. NP_o indicates the total open probability for all NAN-IAV channels during one whole-cell recording. After the whole-cell recording was conducted for 10 s, we chose a time window of 10 s to calculate the NP_o. Then, the NP_o for each recording was computed in Clampfit 10.5 software.

Immunohistochemistry. For neurobiotin staining, after whole-cell recording of lch1 neurons, *Drosophila* larvae were fixed for 20 min in 4% paraformaldehyde (PFA) in PBS, permeabilized in PBST (0.2% Triton-X in PBS) for 20 min, blocked in 5% bovine serum albumin for 20 min, and then washed for 30 min. Then, the larvae were incubated with 1:1,000 streptavidin-Cy3 for 1 h at room temperature. Finally, the larvae were washed for 20 min in PBST. Images were acquired with an Olympus FV1200 confocal microscope using a 40× oil-immersion objective.

For GFP staining, dissected *Drosophila* larvae were fixed for 20 min in 4% PFA in PBS, blocked for 20 min, incubated in rabbit anti-GFP (1:300) for 12 h at 4 °C, and then incubated in Alexa Fluor 488 Donkey anti-Rabbit (1:200) for 2 h at room temperature. Finally, the larvae were washed for 20 min in PBST.

For all the stained larvae, images were acquired with an Olympus FV1200 confocal microscope using a 40× oil-immersion objective.

For *Drosophila* S2 cell staining, we used a PCR-based approach to introduce the in-frame fused myc-tag (EQKLISEEDL) behind the Q455 site of IAV. The pUAST-455myc-IAV-mCherry and pUAST-NAN-Flag constructs were cotransfected with pActin-Gal4. A total of 36 to 48 h after transfection, cells were plated onto ConA-coated coverslips for staining. The primary antibody (mouse anti-myc-tag, Cell Signaling 2276) was diluted 1:200 in Schneider's *Drosophila* Medium and incubated with transfected cells for 30 min at 25 °C. After fixation with 4% PFA for 30 min at 4 °C, the cells were blocked for 30 min at room temperature and then incubated with the secondary antibody (goat anti-mouse Alexa488, 1:500, Jackson ImmunoResearch) for 30 min.

Mechanical and Sound Stimulation. A glass probe was driven by a piezo actuator mounted on a micromanipulator to give mechanical stimulation. The movements were triggered and controlled by the piezo controller, which is synchronized with the programmed signals from pClamp software. For larval Cho neuron stimulation to induce electrophysiological responses, the stimulation pipette was sealed and polished to a diameter of ∼10 μm. The probe moved along an angle of ∼45° to the tip of lch1 neuron dendrites. For the S2 cells recording, the stimulation pipette was sealed and polished to a diameter around 1 μm. A series of 400-ms mechanical steps in 2-μm increments were applied to whole-cell clamped cells. Pure tones (500 Hz) were synthesized in MATLAB (Mathworks). Sounds were delivered through a speaker positioned ∼20 cm from the larvae fillet preparation, where we placed the sound level meter to measure the sound levels.

High-Speed Pressure Clamp. An outside-out patch was used for studying the stretch-activated currents in S2 cells (7). Negative and positive pressures were applied to the excised membrane via a High-Speed Pressure Clamp (HSPC, ALA Scientific). Controlling signals generated from Clampex software were sent to HSPC to adjust the timing and intensity of the pressures. Pressure steps of 400 ms with 20 mmHg increment were applied to the excised membrane through the recording pipette.

Data Analysis. To measure the activation and adaptation time constants of MET currents in lch1 neurons, we used monoexponential fits for the activation and adaptation phase of the currents according to the equation $I = A \exp(-t/\tau) + C$.

To determine the total excitatory charge influx from the MET current (Fig. 7*G*), the area under the "on" current response curve was obtained by the integration method. After adjusting the baseline to zero using Clampfit, we calculated the integral in general by direct summation of $I(t_k)\,\Delta t_k$, where $I(t_k)$ is the current amplitude at the time point t_k and Δt_k is the sampling interval.

To calculate the reversal potentials for spontaneous NAN-IAV channels, each cell in each solution was held with voltage steps ranging from −100 mV to 100 mV with 20-mV increments. The single-channel amplitude was obtained from the amplitude histograms. The channel conductance for each voltage step was calculated from the current amplitude. Then, the reversal potentials were determined from fitting of the I–V curves. The measured liquid junction potentials for Na^+/K^+, Na^+/Cs^+, K^+/Cs^+, and Ca^{2+}/Cs^+ were respectively observed to be +4.5 mV, +4.9 mV, +0.6 mV, and +9.7 mV. To estimate the relative permeability ratio of P_X/P_Y for monovalent cations, we used the following equation derived from the Goldman–Hodgkin–Katz model as previously described:

$$E_{rev} = \frac{RT}{zF} \ln \frac{P_X[X]_{out}}{P_Y[Y]_{in}},$$

where E_{rev} is the reversal potential of the current. To calculate the permeability ratio for Ca^{2+}/Cs^+, the following equation was used:

$$E_{rev} = \frac{RT}{zF} \ln \left(\sqrt{\frac{1}{4} + \frac{4P_{Ca^{2+}}[Ca^{2+}]_{out}}{P_{Cs^+}[Cs^+]_{in}}} - \frac{1}{2} \right).$$

The single-channel conductance was then calculated as

$$\gamma = i/(V_m - E_{rev}),$$

where V_m is the holding potential, i is the single-channel current amplitude, and E_{rev} is the reversal potential of the current.

Statistical Analysis. The Statistical Program for Social Sciences 22.0 (IBM Inc.) and GraphPad Prism 8 (GraphPad Software) were used for statistical analysis and graph generation. The data are shown as the mean value ± SEM.

Data Availability. All study data are included in the article and/or *SI Appendix*.

ACKNOWLEDGMENTS. We thank Yuh Nung Jan (University of California, San Francisco) and Yongqing Zhang (Institute of Genetics and Developmental Biology, Chinese Academy of Sciences) for the vector and fly lines. We also thank the Core Facility of *Drosophila* Resource and Technology (Shanghai Institutes of Biological Sciences, Chinese Academy of Sciences) for the fly microinjections. This research was supported by funds from the National Natural Science Foundation of China (Grant 31571083 and Grant 31970931), the National Key R&D Program of China Project (Grant 2017YFA0103900 and Grant 2016YFA0502800), the Program for Professor of Special Appointment (Eastern Scholar of Shanghai, Grant TP2014008), the Shanghai Municipal Science and Technology Major Project (Grant 2018SHZDZX01), Zhangjiang Laboratory (ZJLab) and the Shanghai Center for Brain Science and Brain-Inspired Technology, and the Shanghai Rising-Star Program (Grant 14QA1400800).

1. J. T. Albert, M. C. Göpfert, Hearing in Drosophila. *Curr. Opin. Neurobiol.* **34**, 79–85 (2015).
2. D. F. Eberl, R. W. Hardy, M. J. Kernan, Genetically similar transduction mechanisms for touch and hearing in Drosophila. *J. Neurosci.* **20**, 5981–5988 (2000).
3. A. Kamikouchi *et al.*, The neural basis of Drosophila gravity-sensing and hearing. *Nature* **458**, 165–171 (2009).
4. Y. Sun *et al.*, TRPA channels distinguish gravity sensing from hearing in Johnston's organ. *Proc. Natl. Acad. Sci. U.S.A.* **106**, 13606–13611 (2009).
5. S. Yorozu *et al.*, Distinct sensory representations of wind and near-field sound in the Drosophila brain. *Nature* **458**, 201–205 (2009).
6. Z. Gong *et al.*, Two interdependent TRPV channel subunits, inactive and Nanchung, mediate hearing in Drosophila. *J. Neurosci.* **24**, 9059–9066 (2004).
7. Z. Yan *et al.*, Drosophila NOMPC is a mechanotransduction channel subunit for gentle-touch sensation. *Nature* **493**, 221–225 (2013).
8. J. Kim *et al.*, A TRPV family ion channel required for hearing in Drosophila. *Nature* **424**, 81–84 (2003).
9. K. Venkatachalam, C. Montell, TRP channels. *Annu. Rev. Biochem.* **76**, 387–417 (2007).
10. M. C. Göpfert, J. T. Albert, B. Nadrowski, A. Kamikouchi, Specification of auditory sensitivity by Drosophila TRP channels. *Nat. Neurosci.* **9**, 999–1000 (2006).
11. T. Effertz, R. Wiek, M. C. Göpfert, C. Nomp, NompC TRP channel is essential for Drosophila sound receptor function. *Curr. Biol.* **21**, 592–597 (2011).
12. T. Effertz, B. Nadrowski, D. Piepenbrock, J. T. Albert, M. C. Göpfert, Direct gating and mechanical integrity of Drosophila auditory transducers require TRPN1. *Nat. Neurosci.* **15**, 1198–1200 (2012).
13. B. P. Lehnert, A. E. Baker, Q. Gaudry, A. S. Chiang, R. I. Wilson, Distinct roles of TRP channels in auditory transduction and amplification in Drosophila. *Neuron* **77**, 115–128 (2013).
14. W. Zhang, Z. Yan, L. Y. Jan, Y. N. Jan, Sound response mediated by the TRP channels NOMPC, NANCHUNG, and INACTIVE in chordotonal organs of Drosophila larvae. *Proc. Natl. Acad. Sci. U.S.A.* **110**, 13612–13617 (2013).
15. D. P. Corey, A. J. Hudspeth, Ionic basis of the receptor potential in a vertebrate hair cell. *Nature* **281**, 675–677 (1979).
16. G. S. Géléoc, J. R. Holt, Developmental acquisition of sensory transduction in hair cells of the mouse inner ear. *Nat. Neurosci.* **6**, 1019–1020 (2003).
17. P. G. Gillespie, U. Müller, Mechanotransduction by hair cells: Models, molecules, and mechanisms. *Cell* **139**, 33–44 (2009).
18. A. J. Hudspeth, D. P. Corey, Sensitivity, polarity, and conductance change in the response of vertebrate hair cells to controlled mechanical stimuli. *Proc. Natl. Acad. Sci. U.S.A.* **74**, 2407–2411 (1977).
19. A. J. Ricci, A. C. Crawford, R. Fettiplace, Tonotopic variation in the conductance of the hair cell mechanotransducer channel. *Neuron* **40**, 983–990 (2003).
20. W. Xiong *et al.*, TMHS is an integral component of the mechanotransduction machinery of cochlear hair cells. *Cell* **151**, 1283–1295 (2012).
21. K. G. Hill, The physiology of locust auditory receptors I. Discrete depolarisations of receptor cells. *J. Comp. Physiol.* **152**, 475–482 (1983).
22. B. Warren, T. Matheson, The role of the mechanotransduction ion channel candidate Nanchung-Inactive in auditory transduction in an insect ear. *J. Neurosci.* **38**, 3741–3752 (2018).
23. A. J. Ricci, H. J. Kennedy, A. C. Crawford, R. Fettiplace, The transduction channel filter in auditory hair cells. *J. Neurosci.* **25**, 7831–7839 (2005).
24. D. P. Corey, A. J. Hudspeth, Response latency of vertebrate hair cells. *Biophys. J.* **26**, 499–506 (1979).
25. L. Kang, J. Gao, W. R. Schafer, Z. Xie, X. Z. Xu, *C. elegans* TRP family protein TRP-4 is a pore-forming subunit of a native mechanotransduction channel. *Neuron* **67**, 381–391 (2010).
26. A. Upadhyay *et al.*, Nicotinamide is an endogenous agonist for a *C. elegans* TRPV OSM-9 and OCR-4 channel. *Nat. Commun.* **7**, 13135 (2016).
27. E. Cao, M. Liao, Y. Cheng, D. Julius, TRPV1 structures in distinct conformations reveal activation mechanisms. *Nature* **504**, 113–118 (2013).
28. M. Liao, E. Cao, D. Julius, Y. Cheng, Structure of the TRPV1 ion channel determined by electron cryo-microscopy. *Nature* **504**, 107–112 (2013).

29. C. H. Liu *et al.*, In vivo identification and manipulation of the Ca^{2+} selectivity filter in the Drosophila transient receptor potential channel. *J. Neurosci.* **27**, 604–615 (2007).
30. Y. Yu *et al.*, Molecular mechanism of the assembly of an acid-sensing receptor ion channel complex. *Nat. Commun.* **3**, 1252 (2012).
31. N. Bavi *et al.*, The role of MscL amphipathic N terminus indicates a blueprint for bilayer-mediated gating of mechanosensitive channels. *Nat. Commun.* **7**, 11984 (2016).
32. P. Jin *et al.*, Electron cryo-microscopy structure of the mechanotransduction channel NOMPC. *Nature* **547**, 118–122 (2017).
33. W. Zhang *et al.*, Ankyrin repeats convey force to gate the NOMPC mechanotransduction channel. *Cell* **162**, 1391–1403 (2015).
34. P. Zhou, M. M. Polovitskaya, T. J. Jentsch, LRRC8 N termini influence pore properties and gating of volume-regulated anion channels (VRACs). *J. Biol. Chem.* **293**, 13440–13451 (2018).
35. X. Liang *et al.*, A NOMPC-dependent membrane-microtubule connector is a candidate for the gating spring in fly mechanoreceptors. *Curr. Biol.* **23**, 755–763 (2013).
36. D. Zanini, M. C. Göpfert, Mechanosensation: Tethered ion channels. *Curr. Biol.* **23**, R349–R351 (2013).
37. L. Sun *et al.*, Ultrastructural organization of NompC in the mechanoreceptive organelle of *Drosophila* campaniform mechanoreceptors. *Proc. Natl. Acad. Sci. U.S.A.* **116**, 7343–7352 (2019).
38. J. Arnadóttir, M. Chalfie, Eukaryotic mechanosensitive channels. *Annu. Rev. Biophys.* **39**, 111–137 (2010).
39. C. Kung, A possible unifying principle for mechanosensation. *Nature* **436**, 647–654 (2005).
40. S. S. Ranade, R. Syeda, A. Patapoutian, Mechanically activated ion channels. *Neuron* **87**, 1162–1179 (2015).
41. M. A. Vollrath, K. Y. Kwan, D. P. Corey, The micromachinery of mechanotransduction in hair cells. *Annu. Rev. Neurosci.* **30**, 339–365 (2007).
42. M. Zhang *et al.*, Structure of the mechanosensitive OSCA channels. *Nat. Struct. Mol. Biol.* **25**, 850–858 (2018).
43. S. E. Murthy *et al.*, OSCA/TMEM63 are an Evolutionarily Conserved Family of Mechanically Activated Ion Channels. *eLife.* **7**, e41844 (2018).
44. Y. Wang *et al.*, The push-to-open mechanism of the tethered mechanosensitive ion channel NompC. *eLife* **10**, e58388 (2021).
45. S. G. Brohawn, E. B. Campbell, R. MacKinnon, Physical mechanism for gating and mechanosensitivity of the human TRAAK K+ channel. *Nature* **516**, 126–130 (2014).
46. J. Ge *et al.*, Architecture of the mammalian mechanosensitive Piezo1 channel. *Nature* **527**, 64–69 (2015).
47. Y. R. Guo, R. MacKinnon, Structure-based membrane dome mechanism for Piezo mechanosensitivity. *eLife* **6**, e33660 (2017).
48. K. Saotome *et al.*, Structure of the mechanically activated ion channel Piezo1. *Nature* **554**, 481–486 (2018).
49. R. Syeda *et al.*, Piezo1 channels are inherently mechanosensitive. *Cell Rep.* **17**, 1739–1746 (2016).
50. C. D. Cox *et al.*, Removal of the mechanoprotective influence of the cytoskeleton reveals PIEZO1 is gated by bilayer tension. *Nat. Commun.* **7**, 10366 (2016).
51. R. G. Kavlie, J. T. Albert, Chordotonal organs. *Curr. Biol.* **23**, R334–R335 (2013).
52. J. C. Tuthill, R. I. Wilson, Mechanosensation and adaptive motor control in insects. *Curr. Biol.* **26**, R1022–R1038 (2016).
53. M. J. Kernan, Mechanotransduction and auditory transduction in Drosophila. *Pflugers Arch.* **454**, 703–720 (2007).
54. G. Chang, R. H. Spencer, A. T. Lee, M. T. Barclay, D. C. Rees, Structure of the MscL homolog from Mycobacterium tuberculosis: A gated mechanosensitive ion channel. *Science* **282**, 2220–2226 (1998).
55. J. Li *et al.*, Mechanical coupling of the multiple structural elements of the large-conductance mechanosensitive channel during expansion. *Proc. Natl. Acad. Sci. U.S.A.* **112**, 10726–10731 (2015).
56. Z. Liu, C. S. Gandhi, D. C. Rees, Structure of a tetrameric MscL in an expanded intermediate state. *Nature* **461**, 120–124 (2009).
57. S. R. Olsen, V. Bhandawat, R. I. Wilson, Excitatory interactions between olfactory processing channels in the Drosophila antennal lobe. *Neuron* **54**, 89–103 (2007).
58. A. W. Azevedo, R. I. Wilson, Active mechanisms of vibration encoding and frequency filtering in central mechanosensory neurons. *Neuron* **96**, 446–460.e9 (2017).
59. E. Neher, Correction for liquid junction potentials in patch clamp experiments. *Methods Enzymol.* **207**, 123–131 (1992).